Tuijin Jishu/Journal of Propulsion Technology
ISSN: 1001-4055
Vol. 44 No. 3 (2023)

Design and Construction of a Continous Stirring Hydrothermal Liquefaction Batch Reactor

Obiora Nnaemeka Ezenwa[1,2*], Chinedum Ogonna Mgbemena[2], Eyere Emagbetere[2]
[1]Nnamdi Azikiwe University, Awka, Anambra State, Nigeria.
[2]Federal University of Petroleum Resources Effurun, Delta State, Nigeria
Corresponding Author: Obiora Nnaemeka Ezenwa
Email: on.ezenwa@unizik.edu.ng

Abstract:

The design and construction of a hydrothermal liquefaction (HTL) machine play a crucial role in the development of renewable energy technologies and the utilization of biomass resources. This work focused on the design and production of continuous stirring hydrothermal liquefaction batch reactor. The reactor comprises of various components, such as the supporting frame on which the reactor seats for easy operation, the reaction chamber with heating elements, the reactor housing, pressure gauge and valve, gas tank, electric motor, voltage regulator, and the control box. The reactor was designed based on the liquefaction temperature of 500°C, and pressure of 240 bar, with the reaction chamber volume of 0.001m^3, for laboratory purposes. The materials used for the production the reactor was carefully selected based on the designed parameters, and locally sourced for cost effectiveness. Performance evaluation test was conducted on the reactor using beet pulp at the reaction temperature of 250°C, water biomass ratio of 8.5 and a heating rate of 10°C/min, for 20 minutes, a bio oil and solid residue yield of 19 and 35% was recorded which is closely related to result reported in the literature. Hence, this reactor can be used to investigate the potentials of producing bio oil from wet biomass through hydrothermal liquefaction process.

Keywords: Hydrothermal Liquefaction, Biomass, Bio Oil, Solid Residue, Reaction Temperature, Heating Rate.

1. Introduction

The 21st century has continued to experience increase in global demand for energy, due to rapid increase in population and economic growth, especially in large emerging countries (Nada and Alrikabi, 2014). This has led to overdependence on fossil fuels for energy generation. Consumption of fossil fuels accounts for 85 percent of the energy we use on earth today. Its usage is basically on transport and power generation applications, which cannot be sustained over a long period due to its non-renewable nature. Being a non-renewable energy source, they are destined to deplete in the near future because they are not replenished at the speed with which they are consumed. Fossil fuel is associated with so many issues such as climate change, air pollution, water pollution, environmental degradation (Savannah, 2021). To address these issues and transition to a more sustainable energy system, there is a growing need for alternative sources of energy, such as biomass energy. Biomass refers to organic matter derived from plants, animals, and their byproducts. The methods for biomass conversion into biofuels, which are capable of substituting petroleum-derived fuels, are complex and ranges from biochemical conversion processes to severe catalytic thermochemical processes. However, bio-oil as a form of biofuel which are produced through thermochemical processes, either pyrolysis, or liquefaction processes.

Hydrothermal liquefaction offers several advantages that makes it an attractive option for an efficient biomass conversion over other thermochemical conversion techniques because, it does not require prior thermal drying and thus results in cost reductions for wet materials, and suitable for the production of bio-oil from biomass with varying moisture contents. Secondly, it uses hot pressurized water as a reaction medium, hence, other chemicals may not be necessary. Thirdly, HTL is less corrosive to equipment than other conversion alternatives, and the

whole process is versatile and environmentally friendly (Cao et al, 2017). Furthermore, HTL has great potential due to its flexibility in the conversion of different categories of biomass feedstocks such as aquatic wastes, lignocellulosic biomass, herbaceous matter, food-processing wastes, fungus, cyanobacteria, and biochemical wastes from macro/microorganisms (Sahu et al, 2020).

Hydrothermal liquefaction (HTL) is the thermochemical process of converting a broad range of biomass types into bio-oil in the presence of hot compressed water at subcritical conditions. HTL requires operating temperature of 300 °C to 350 °C at a pressure of 5 MPa to 20 MPa for 5mins to 60 mins, wherein water is in the liquid form. It mimics the processing of fossil fuels buried deep inside the earth, but occurs in minutes or hours.

However, one of the major challenges facing the utilization of biomass through hydrothermal liquefaction is the advancement of technology for efficient and sustainable bio-oil production. The two major type of reactors available for HTL are the continuous reactors and batch reactors.

In continuous HTL reactors, the sample is directly subjected to the desired temperature and for the required time. The retention time is controlled by the length of the reactor and flow rate of the feedstock slurry (Eillott et al, 2015). A typical continuous HTL reactor as seen in figure 1, consist of a feed tank, high-pressure metering pump, coil preheater, vertical plug-flow reactor, dual inline filters, cooling coil heat exchanger, back-pressure regulator, and product tank.

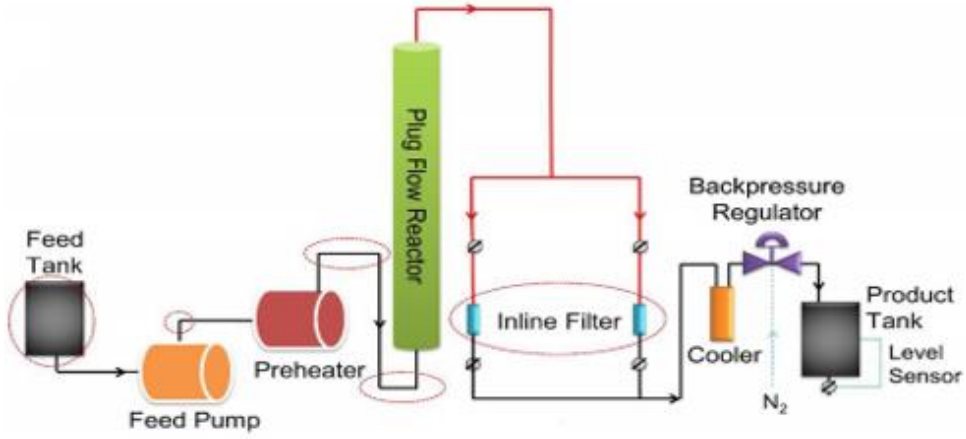

Figure 1: Schematic diagram of a pilot scale continuous flow reactor (Cheng et al, 2019)

In this type of reactor, the slurry is pumped into the tube by a feed pump, through some type of external heat source. The major benefit of this type of reactor is greater temperature control and the ability to achieve higher heating rates due to an increased tubing surface area and thinner reactor walls. However, at a low flow rates (laminar conditions) the slurry experiences frictional drag forces that slow the media near the internal tubing surface. This often leads to excessive heating and slurry charring on the tubing walls with unreacted material in the center, also to achieve a very high processing temperatures (>350 °C) very long sections of tubing must be employed which further increases the reactor complexity and material costs. More so, continuous HTL reactors have limitations on the solid load of the feedstock because if exceeded, it becomes difficult to pump the slurry in the system (Cheng et al, 2019).

But, a typical HTL batch reactor, as seen figure 2, employs a sealed stainless autoclave which is heated from the outside-in by a resistance wire heater connected to an external temperature controller.

In this type of reactor, the sample is heated inside from room temperature to the desired temperature. This forces the sample to go through all the temperature range until the desired temperature is achieved instead of subjecting the sample directly to the desired temperature. The same issue is encountered during the cooling part of the process as the reactor is shut down after the desired retention time is completed and it is left to cool down to room temperature without any intervention resulting in additional time of heat energy and the selected retention time. This makes it hard to separate the effects of temperature and retention time. However, Overend and Chornet's

severity index can help to combine the effect of these two parameters into one (Kiran et al, 2018). Also a batch reactor with fast heating as demonstrated by Faeth et al, shows a method called as Fast HTL which might be closer to conditions in the continuous system that used faster heating rates and lower retention time in the batch experiment and produced significantly higher yields in comparison to conventional method (Faeth et al, 2013). Another limitation of the batch reactors is scalability. However, batch experiments give a good idea of products and conditions of the HTL process, thus providing a good starting point for understanding HTL mechanism. Hence the reason for the selection of for production of this type of reactor for laboratory purposes.

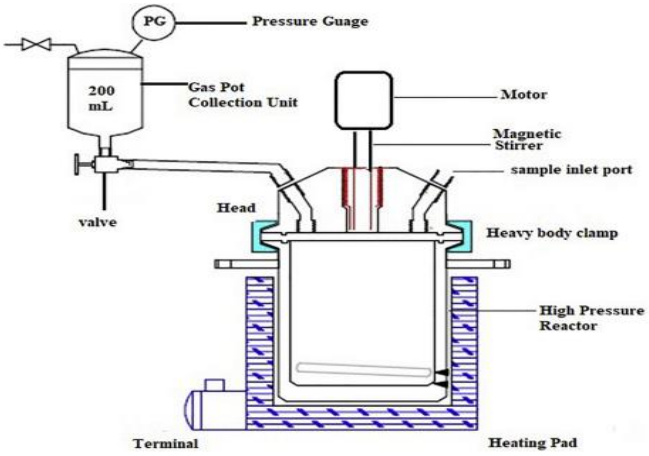

Figure 2: Schematic diagram of HTL reactor (Kiran et al, 2018)

2. Methods

The development of the reactor was done by carrying out the graphic and mathematical design of the reactor. The design was simulated to ensure safe operations. The fabrication was done using selected materials according to the design specifications.

2.1 Graphic Design

The HTL reactor, which comprises of different components, such as supporting frame, reactor housing, reaction chamber, reactor gas tank, and electrical components of the reactor, was modeled using Solidworks software, version 10. The components were first drawn in parts, and then assembled by mating the parts. The materials and colour to be used for the reactor, is then selected from Solidworks' vast library and applied to the parts. The result of the graphics is presented in the next chapter.

2.2 Mathematical Design

Mathematical design was done to determine some of the parameters that will guide the selection of materials for the production of the reactor to ensure safe and smooth operations.

2.2.1 Volume and Height of the Reaction Chamber

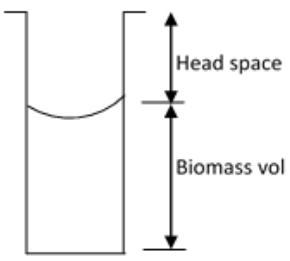

Figure 3: Schematic diagram, showing the volume of the reactor

From the design consideration, the volume of wet biomass (V_{wb}) was considered, hence the volume (V_r) and height (h_r) of the reaction chamber, considering 30% head space as seen in figure 3, will be given by equation (1) and (2) respectively as;

$$V_r = V_{wb} + 0.3\,(V_{wb}) \quad (1)$$

$$V_r = \pi \left(\frac{d_r}{2}\right)^2 h_r \quad (2)$$

Where d_r is the diameter of the reaction chamber.

2.2.2 Reaction Chamber Wall Thickness

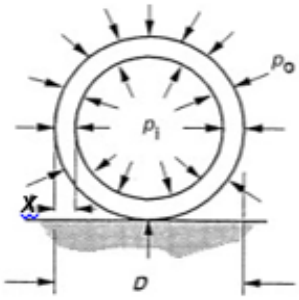

Figure 4: Schematic diagram, showing the cross section of the reaction chamber

Considering figure 3.2, P_i is the internal pressure developed within the reaction chamber, P_o is the atmospheric pressure acting on the surface, while d_r and x is the diameter and the thickness of the reaction chamber. To calculate the wall thickness of the reaction chamber, the type of stainless steel to be used is considered, in order to determine the thickness that will withstand the maximum working pressure and temperature. This was done using equation (3)

$$\sigma_h = (P_i - P_o)\frac{d_r}{2x} \times f_s \quad \text{(Bai et al, 2014)} \quad (3)$$

Where σ_h is the hoop stress, and it's been replaced with ultimate tensile strength during theoretical calculations (Reddy, 2005), and f_s is the factor of safety.

2.2.3 Heating Capacity

The wattage of the heating element to obtain the maximum heating rate is given;

$$E = \frac{mCp\Delta T}{t} \quad (4)$$

Where E is the Wattage (watt) of the heating element,

Cp is the specific heat of the reactor material obtained from ASTM metal table chart,

ΔT is change in temperature between the desired maximum temperature (T_1) and the temperature of the environment (T_2), given by the expression;

$$\Delta T = (T_1 - T_2) \quad (5)$$

t is the required time to raise the temperature, and m is the mass of the reaction chamber material to be heated up, given by;

$$\rho = \frac{m}{V} \quad (6)$$

Where ρ is the density of the reactor material obtained from ASTM metal table chart, and v is the volume of the reaction chamber material used for the required volume, and it's given by;

$$V = \left(2\pi r_r h_r + 2\pi {r_r}^2\right)x \quad (7)$$

Where r_r is the radius of the reaction chamber.

2.2.4 Thermal Insulation Thickness

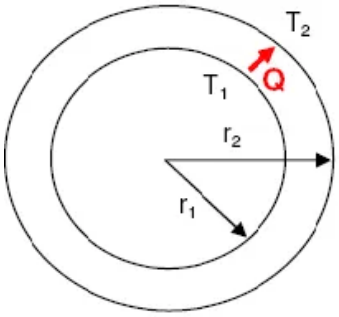

Figure 5: Schematic diagram, showing the cross section of the reactor housing

The thermal insulation thickness of the lagged wall thickness was determined in consideration with the lagging material to ensure adequate prevention of heat loss. Considering figure 5, which shows the cross section of the reactor housing, r_1 and r_2 is the internal and external radius of the reactor housing respectively, $T_{r1}$and T_{r2} is the temperature within and the expected temperature outside the reactor housing, respectively. While Q is the quantity of heat supplied within the reactor housing. Therefore to determine the insulation thickness, r_2 will be calculated using equation (8), since the internal radius of the reactor housing is known.

$$Q = \frac{(T_{r1} - T_{r2})}{In\left(\frac{r_2}{r_1}\right)/(2\pi K h_{rh})} \quad (8)$$

Where K the thermal conductivity of the lagging material, and h_{rh} is the height of the reactor housing.

Hence the insulation thickness (X_L) was calculated using equation (9);

$$x_L = (r_2 - r_1) \quad (9)$$

2.3 Fabrication

The fabrication of the reactor was done in accordance with standard fabrication process, which entails marking and cutting of the acquired materials to the required shape and size, drilling of required holes to the specified dimensions, joining of the cut out materials by welding to obtain the desired components, surfacing finishing of the produced component by grinding of excess weld deposit, filling of the edges for smoothness, sandpapering of the surfaces to remove rust and impurities, and spray painting to prevent rust and improve aesthetic purposes, and assembling of the produced component with bolts and nuts according to the production drawing.

2.4 Test and Evaluation

The reactor was test through hydrothermal liquefaction of beet pulp. The liquefaction condition was chosen from the work reported by Brilman et al (2017) at the temperature of 250 ^{o}C and residence time of 10 mins. The water-biomass ratio used was 8.5 according to the method reported by Brilman et al (2017). After the reaction, and the products separation, the yields were determined as follows;

$$\%Yield_{BO} = \frac{Mass\ of\ LIght\ Oil}{Mass\ of\ Biomass} \times 100 \quad (10)$$

$$\%Yield_{SR} = \frac{Mass\ of\ Solid\ Residue}{Mass\ of\ Biomass} \times 100 \quad (11)$$

$$\%Yield_{gas\ \&\ water} = 100\% - \%Yield_{LO} - \%Yield_{SR} \quad (12)$$

Where $\%Yield_{BO}$, $\%Yield_{SR}$, $\%Yield_{gas\ \&\ water}$ are the percentage weight yield for bio oil, solid residue and gaseous product respectively. The yields where compared to that reported by Brilman et al (2017), under the same condition.

3. Results and Discussion

3.1 Graphics Design Result

Figure 6: Graphics model of the designed reactor

The graphics model the designed reactor and its components are shown in figure 6. (a) Assembled reactor. (b) The supporting frame on which the reactor and its components seats. (c) The reactor housing, which houses the reaction chamber, and also serves as the heating chamber. (d) The gas tank, where the gaseous product is being emptied. (e) The reaction chamber with heater wound round the outer which supplies the heat for the reaction. (f) The reaction chamber cover with stirrer and pressure gauge that stirs and reads the pressure as the reaction proceeds. (g) The control box that houses all the electrical components such the thermocouple and the magnetic contactor. And (f) the voltage regulator that regulates the heating rate.

3.2 Mathematical Design Results

Table 1: The reactor parameters obtain from the mathematical design

Reactor Parameter	Symbol	Quantity	Unit	Source
Volume of wet biomass	V_{wb}	0.0012	m^3	Considered
Volume of reaction chamber	V_r	0.0016	m^3	Equation (1)
Diameter of the reaction chamber	d_r	0.102	m	Considered to allow for stirrer.
Height of the reaction chamber	h_r	0.2	m	Equation (2)
Maximum internal pressure	P_i	4	MPa	Considered, liquefaction Pressure range
External Pressure	P_o	0.101325	MPa	Atmospheric pressure

Hoop stress	σ_h	505	MPa	Aerospace Specification Metal Inc. (ASM)
Reaction chamber wall thickness	x	5	mm	Equation (3)
Volume of the reaction chamber material	V_{rm}	0.000402	m^3	Equation (6)
Density of the reaction chamber wall material	ρ_{rm}	8000	Kg/m^3	Aerospace Specification Metal Inc. (ASM)
Mass of reaction chamber material	m_{rm}	3.216	kg	Equation (5)
Specific heat capacity of stainless steel	c_p	502.416	J/Kg-K	Aerospace Specification Metal Inc. (ASM)
Change in temperature between the desired and atmospheric temperature	ΔT	473	^oC	Equation (5)
Time required to reach maximum temperature	t	10	mins	Considered
Heater capacity	E	2	KW	Equation (4)
Maximum desired temperature	T_1	500	^oC	Considered, liquefaction temperature range
Thermal conductivity of lagging material	K	0.48	$Wm^{-1}K^{-1}$	Mgbemena et al, (2019)
Height of reactor housing chamber	r_{rh}	0.33	m	Considered to house the reaction chamber
Internal radius of the reactor housing	r_1	0.102	m	Considered
External radius of the reactor housing	r_2	0.15	m	Equation (8)
Thermal insulation thickness	X_L	0.1	m	Equation (9)

The result of the mathematical design of the reactor is shown in table 1. Some of the parameters such as the maximum working temperature was considered based on the reported liquefaction parameters as seen in Marulanda et al, (2019); Anamika et al (2022). Some other considered parameter was done for easy of fabrication and operation. Parameters such as thermal conductivity specific heat capacity and other parameters that describe the properties of some the materials used were obtained from available literature as reported in the table 1. While the rest of the other parameters was calculated using the quoted equations as described in section 2.2, to enable the fabrication of functional and reliable reactor.

3.3 Thermal Distribution and Static Stress Simulation Result

Thermal distribution analysis of the reactor housing is shown in figure 7, to ascertain the adequacy of the determined insulation. It can been from the figure that the chosen insulation thickness and materials is sufficient to properly lag the reactor housing to prevent heat loss. Also the static stress simulation of the reaction chamber is shown in figure 8. This simulation is of essence to ascertain whether the determined reaction chamber wall thickness will be sufficient enough to withstand the thermal and mechanical stress that will be subjected to it with

respect to the chosen material for the reaction chamber. The simulation result recorded a maximum exerted stress of 5.964 x 10^8 N/m^2 within the reaction chamber, which is lesser than the yield strength (6.204 x 10^8 N/m^2) of the chosen material and its thickness as shown in the Von Mises stress indication bar of figure 8. This shows that the design is adequate for the production of the reactor's reaction chamber.

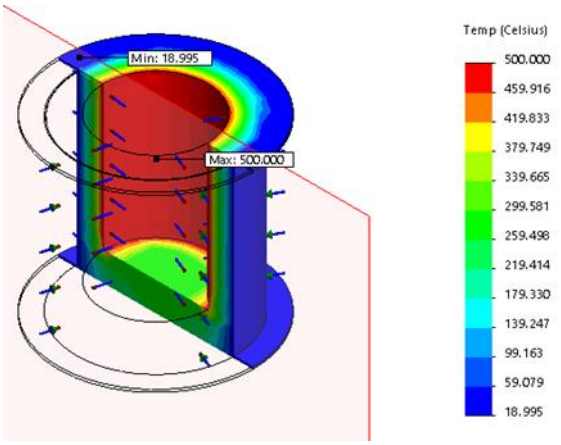

Figure 7: Simulated model showing thermal distribution along reactor housing walls

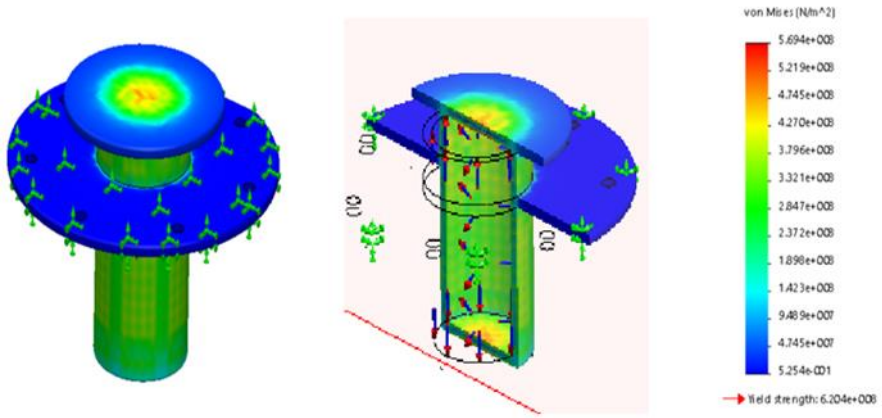

Figure 8: Static stress simulation analysis result of the reaction chamber

3.4 Developed Reactor and its Operation

The produced hydrothermal liquefaction reactor is shown in figure 9. It is been operated by arranging the components as seen in the figure. The reactant is placed inside the reaction chamber and properly locked with either, bolt and nut, or with high torque clamp, with a high heat resistant Teflon material placed in between the reactor flange and cover to prevent pressure leakage. The reactor is connected to mains which supplies power to the reactor through the voltage regulator. Set the voltage to the required setpoint that will give the required heating rate, and ensure that the pressure valve is completely closed, until when pressure regulation is needed. The reaction temperature is set at the thermocouple temperature adjustment bottom and the heater is powered on with the heater switch alongside with the stirrer. The reaction proceeds until the reaction time is exceeded, the reactor will be turned off and allowed to cool down before dismantling. Care must be taken to ensure that the gaseous product is completely discharged into the gas tank by opening of the valve before dismantling the clamp.

Figure 9: The picture of the produced reactor

3.5 Calibration Result of the Reactor's Heating Rate

Table 2: Temperature of the reactor at different voltage and time

S/N	t (mins)	T_{140V} (°C)	T_{160V} (°C)	T_{180V} (°C)	T_{200V} (°C)	T_{220V} (°C)	T_{240V} (°C)
1	0	30	30	30	30	30	30
2	2	41	45	48	52	54	59
3	4	50	61	64	72	80	88
4	6	61	75	82	93	105	118
5	8	70	89	100	115	128	148
6	10	79	103	118	138	156	178
7	12	87	115	133	157	181	206
8	14	95	125	149	182	208	234
9	16	101	135	163	198	231	260
10	18	107	142	177	215	248	286
11	20	110	149	187	225	261	305

Table 2, presents the experimental result for the calibration of the reactor's heating rate. This is because the reactor was designed in such a way that its heating rate is regulated with its voltage regulator. The columns labeled T_{140} to T_{240} are the temperature obtained at different voltages from 140 volts to 240 volts at an interval of 20 volts at 2

minutes time intervals for 20 minutes. This results were plotted against time to determine the behavior of the heating element with respect to the supplied voltage.

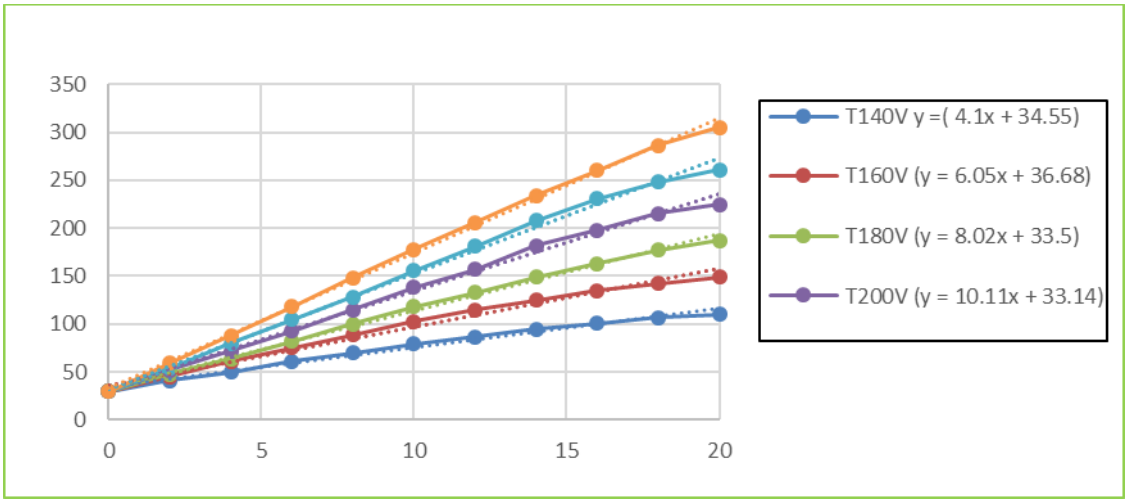

Figure 10: Graph of temperature at different voltages against time

Figure 10, shows the plot the obtained temperature at different voltages against time. The colour code as seen in the plot legend depict the plot at different voltages from 140 volts to 240 at 20 volts interval. It is seen from the graph that the temperature increased linearly with increase in time for all the voltages. The graph also showed that as the voltage increases, temperature increases as expected. These plots were linearized to obtain the equation below that defined the behavior.

Where T_{140V} *to* T_{240V} are the temperatures obtained at different voltages from 140 volts to 240 volts respectively, and t is time interval of the temperature measurement. The slope of the straight line equation which was used to obtain table 3, gives the rate at which the reactor heats at the different voltages.

Table: 3: Table of experimented voltages and the corresponding heating rate.

S/N	V (volts)	R_H (ºC/min)
1	140	4.10
2	160	6.05
3	180	8.02
4	200	10.11
5	220	12.01
6	240	14.04

Table 3, presented the result obtained from linearizing the plots as seen figure 10. The equation generated from the plot gave the heating rate presented table 3 at different voltages, which corresponds to the slope of the plot. This was used to generate a plot that calibrates the reactor's heating rate

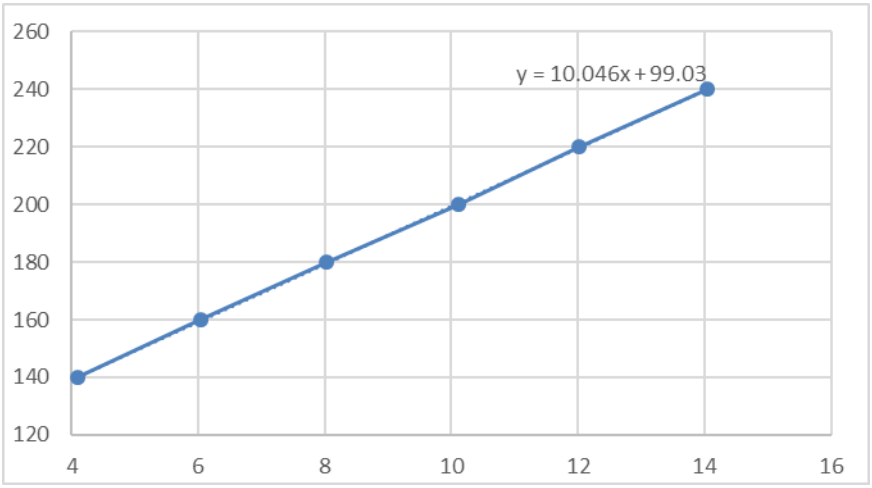

Figure 11: Graph of different voltages and the corresponding heating rate of the reactor.

From the graph it was seen that increase in voltage increases the rate at which the reactor heats in a linear manner. The straight line model generated from this plot as seen on the plot was rearranged to obtain the model that calibrates the reactor's heating as seen in equation (13).

$$R_H = \frac{(V-99.03)}{10.046} \quad (13)$$

This means that for any required heating rate, the calibrated model presented in equation (13) will be used to determine its corresponding setpoint voltage.

3.6 Test Result

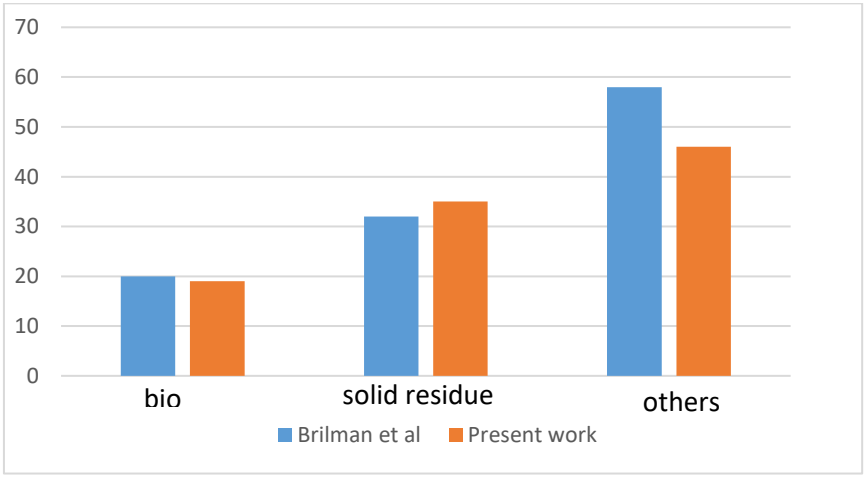

Figure 12: yield result for present work and Brilman et al (2017)

The result of the test performed with the produced reactor is presented in figure 12. The reactor was tested by performing hydrothermal liquefaction of beet pulp using the condition as described by Brilman et al (2017). The result gave a yield that is slightly smaller than that reported by Brilman et al (2017). This can be attributed to the high heating rate of the reactor used by Brilman, which was not been able to be achieved in this work, due to the reaction chamber wall thickness.

4. Conclusions

This work successfully designed and produced a hydrothermal liquefaction reactor for production of bio oil from wet agro waste. The reactor design was simulated with solidworks simulation tool to ensure the adequacy of the design, to prevent failure. The reactor was calibrated to obtain a model that will determine the voltage setpoint

that will give the required heating rate. The produced reactor was tested by carrying out the test according to Brilman et al (2017), which gave a yield result that is slightly smaller than the result reported in Brilman's work, due to the reactors low heating rate. It therefore recommended that future works should consider improving the heating rate of the reactor.

References

[1] Anamika Kushwaha, Ajar Nath Yadav, Brajesh, Singh, Vinay Dwivedi, Satyendra Kumar, Lalit Goswami, Chaudhery Mustanasar Hussain (2022). Life cycle assessment and techno-economic analysis of algae-derived biodiesel: current challenges and future prospects. Waste-to-Energy Approaches Towards Zero Waste Pages 343-372 https://doi.org/10.1016/B978-0-323-85387-3.00003-3

[2] Brilman, D. W. F., Drabik, N., & Wądrzyk, M. (2017). Hydrothermal co-liquefaction of microalgae, wood, and sugar beet pulp. Biomass Conversion and Biorefinery, 7(4), 445–454. doi:10.1007/s13399-017-0241-2

[3] Cheng, F., Le Doux, T., Treftz, B., Woolf, S., Yu, J., Miller, J., Brewer, C. E. (2019). Modification of a pilot-scale continuous flow reactor for hydrothermal liquefaction of wet biomass. MethodsX, 6, 2793–2806. doi:10.1016/j.mex.2019.11.019.

[4] Elliott, D. C., Biller, P., Ross, A. B., Schmidt, A. J., & Jones, S. B. (2015). Hydrothermal liquefaction of biomass: Developments from batch to continuous process. Bioresource Technology, 178, 147–156. doi:10.1016/j.biortech.2014.09.132

[5] Faeth J. L., Valdez P. J., and Savage P. E., (2013). Fast hydrothermal liquefaction of nannochloropsis sp. to produce biocrude. Energy and Fuels, vol. 27, no. 3, pp. 1391– 1398.

[6] Kiran Kumar, P., Vijaya Krishna, S., Verma, K., Pooja, K., Bhagawan, D., Srilatha, K., & Himabindu, V. (2018). Bio oil production from microalgae via hydrothermal liquefaction technology under subcritical water conditions. Journal of Microbiological Methods. doi:10.1016/j.mimet.2018.09.014

[7] Marulanda, V. A., Gutierrez, C. D. B., & Alzate, C. A. C. (2019). Thermochemical, Biological, Biochemical, and Hybrid Conversion Methods of Bio-derived Molecules into Renewable Fuels. Advanced Bioprocessing for Alternative Fuels, Biobased Chemicals, and Bioproducts, 59–81. doi:10.1016/b978-0-12-817941-3.00004-8

[8] Mgbemene, C. A., Akinlabi, E. T., & Ikumapayi, O. M. (2019). Dataset showing thermal conductivity of South-Eastern Nigerian kaolinite clay admixtures with sawdust and iron filings for fired-bricks production. Data in Brief, 27, 104708. doi:10.1016/j.dib.2019.104708

[9] Nada Kh. M. A. Alrikabi, (2014) "Renewable Energy Types," Journal of Clean Energy Technologies vol. 2, no. 1, pp. 61-64.

[10] Sahu, S. N., Sahoo, N. K., Naik, S. N., & Mahapatra, D. M. (2020). Advancements in hydrothermal liquefaction reactors: overview and prospects. Bioreactors, 195–213. doi:10.1016/b978-0-12-821264-6.00012-7

[11] Savannah Bertrand (2021). Fact Sheet | Climate, Environmental, and Health Impacts of Fossil Fuels. Environmental and Energy Study Institute. Retrieved from https://www.eesi.org/papers/view/fact-sheet-climate-environmental-and-health-impacts-of-fossil-fuels-2021